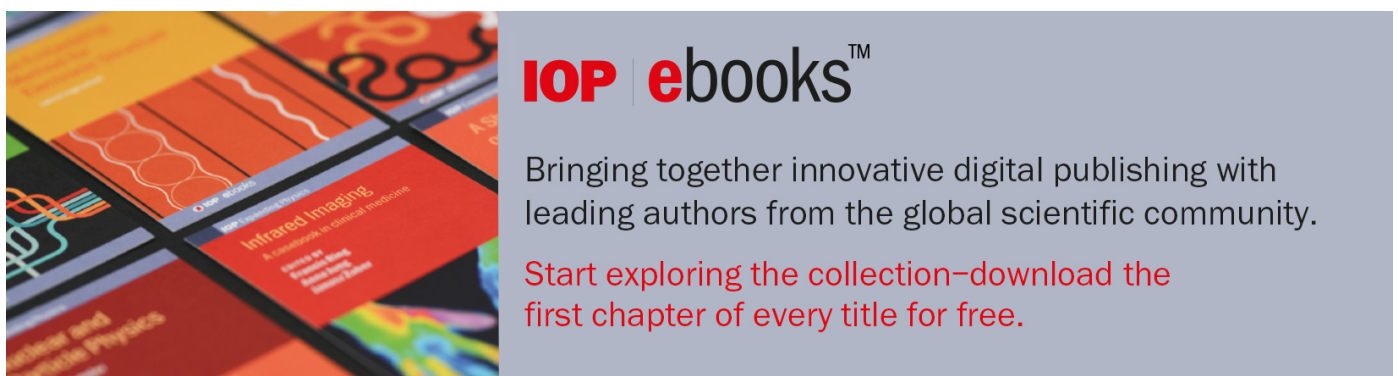


PAPER

## Effect of interfiber bonding on the rupture of electrospun fibrous mats

To cite this article: Poorya Chavoshnejad *et al* 2020 *J. Phys. D: Appl. Phys.* **54** 025302

View the [article online](#) for updates and enhancements.

The image shows a promotional banner for IOP ebooks. On the left, there is a collage of colorful book covers with various scientific and technical designs. On the right, the text reads: "IOP | ebooks™" in a bold, sans-serif font. Below this, it says "Bringing together innovative digital publishing with leading authors from the global scientific community." and "Start exploring the collection—download the first chapter of every title for free." in a smaller font.

**IOP | ebooks™**

Bringing together innovative digital publishing with leading authors from the global scientific community.

Start exploring the collection—download the first chapter of every title for free.

# Effect of interfiber bonding on the rupture of electrospun fibrous mats

Poorya Chavoshnejad<sup>1</sup>, Ohood Alsmairat<sup>1</sup>, Changhong Ke<sup>1,2</sup>  and Mir Jalil Razavi<sup>1</sup> 

<sup>1</sup> Department of Mechanical Engineering, State University of New York at Binghamton, Binghamton, NY 13902, United States of America

<sup>2</sup> Materials Science and Engineering Program, State University of New York at Binghamton, Binghamton, NY 13902, United States of America

E-mail: [mravazi@binghamton.edu](mailto:mravazi@binghamton.edu)

Received 22 June 2020, revised 6 September 2020

Accepted for publication 22 September 2020

Published 19 October 2020



CrossMark

## Abstract

Electrospun fibrous mats have a wide range of applications, and characterizing their mechanical behavior is an important task. In addition to the mechanical properties of the individual fibers, other factors can alter the overall mechanical behavior of the mat. In this study, we use computational and experimental methods to investigate the effect of interfiber bonding on the failure and rupture of typical fibrous mats. A non-linear finite element model of a mat is simulated with randomly distributed fibers with different porosities. The percentage of bonding between intersecting fibers is controlled by an auxiliary code. The results reveal that interfiber bonding increases the stiffness of the mat, and the toughness of the mat increases as well. Interestingly, a large percentage of interfiber bonding at a predefined porosity of a mat does not increase the elastic modulus of the mat, nor does it have considerable effects on the failure behavior. Moreover, the effect of interfiber bonding increases with a mat's porosity. The findings of this study could help tune the mechanical properties of fibrous mats used for different applications.

Keywords: electrospun fibrous mat, interfiber bonding, rupture, finite element

(Some figures may appear in colour only in the online journal)

## 1. Introduction

Electrospinning is an advanced method that can be used to design and fabricate a fibrous structure from nanofibers [1–3]. This method uses a high voltage electric force to produce polymeric fibers with ultrafine diameters ranging from a few nanometers to several micrometers [1, 4]. During electrospinning, a charged polymer jet is deposited onto a grounded collector. Depending on the collector type, stationary or quickly rotating, a mat with randomly oriented fibers or aligned fibers can be created, respectively [5–9]. Unique characteristics such as flexibility, high surface-to-volume ratio, permeability, and absorptivity of the electrospun mats make them ideal for many applications such as composite fibers, filtration structures, wound dressing, catalytic supports, energy harvesting, photonic and electronic devices, drug delivery, and tissue scaffolding [1, 10–14]. The mechanical behavior of a bulk fibrous mat greatly depends on the individual fibers, and

many experimental studies have characterized this dependency according to the non-trivial microstructure [4]. Literature shows that the mechanical properties of an electrospun mat are tunable by changing the characteristics of the polymer [15–17], the diameter of the constituent fibers [18–22], fiber alignment [23], porosity (or fiber packing density) [24–27], and bonding at the cross-points of the fibers [28–30]. Even after considering those parameters, it remains challenging to link the overall bulk material behavior to the small-scale constituent elements. Recently, along with experimental studies, various computational models have tackled this important challenge [4]. Proposed multi-scale modeling techniques (e.g. statistical models, neural networks, molecular dynamics (MD), and finite element) link the behavior of the bulk material to the microstructure architecture [28, 31–35]. Simulations show that the diameter and material behavior of the individual fiber, along with the orientation of fibers, interfiber bonding, the curvature of fibers, and porosity, are all important factors

that have considerable effects on the mechanical properties of fibrous mats. Among the various proposed computational models, the finite element method (FEM) has been widely used in the mechanical characterization of the fibrous nonwoven mats [23, 28, 31, 36–43]. These studies suggest that FEM satisfactorily explains the elastic-plastic behavior of fibrous mats by accounting for the mechanical behavior of the embedded microelements. However, in prior studies, the effect of inter-fiber bonding (fusion) between intersecting fibers on the rupture behavior of fibrous mats has not been discussed very well. Bonding at the cross-points of fibers enhances the mechanical and electrical properties of mats, and it can be induced by thermal treatment [44–47], solvent (or vapor) exposure [48, 49], or covalent cross-linking [50, 51]. In our previous study, using a non-linear FE model, we studied the effect of inter-fiber bonding on the elastic behavior of fibrous mats. The study showed that bonding increases the stiffness of the mat for all ranges of porosities; however, the bonding is more effective at stiffening when the porosity of the mat is low. So far, the presented models for the damage and failure of fibrous mats have mainly focused on the discrete or FE models, without considering the effect of interfiber bonding [40, 42, 52–57]. There are only a few studies that have discussed interfiber bonding and failure of electrospun mats simultaneously [28, 58–60]. Wei *et al* [28] developed a MD model to predict the deformation of an electrospun nanofiber mat by considering the fusion among fibers and the van der Waals interaction. The results of that study showed that the interfiber fusion has a significant effect on the tensile strength of the mat. More fusion points increase the strength of the mat, and over-fusion may reduce the fracture energy. However, this study was in the nanoscale only and not in a multiscale medium, and could not explain why over-fusion does not show a strong influence on the tensile strength. Goutianos *et al* [58] used a 3D finite element model to find the elastic modulus and strength of a fibrous network was mostly controlled by the density and strength of the interfiber bonding. The elastic modulus and strength of the fibrous mat increase as the density and strength of the interfiber bonding increase. Moreover, the mechanical properties of the bonds and their density have a slight effect on the failure strain. Although these models give valuable information, they have limitations that have considerable effects on the overall mechanical behavior of the mat. Individual fibers are modeled by a linear elastic material model before fracture, while in reality, the fibers show an elastic-plastic behavior. The bonding of two fibers is bounded by user-defined lower and upper limits for interaction distances. Lastly, bonding density—the number of bonds in a given area—is a function of the porosity of the mat. In this study, to overcome the aforementioned limitations, we propose a new multiscale finite element model to investigate how interfiber bonding in different porosities can change the rupture behavior of the mat, while the realistic material's microstructure is incorporated explicitly into the model by introducing failure properties of the individual fibers. In the developed model, the numbers of bonded and unbonded cross-points of fibers are controlled deliberately, and they can be independent of the porosity. For tuning the model, the percentage of bonding of all available

cross-points is an average calculated from SEM (scanning electron microscopy) images. Moreover, this study explains the underlying mechanism of the ineffectiveness of the over-fusion in a predefined porosity.

## 2. Methods

### 2.1. Experimental method

The fiber mats used in this study are composed of polymethyl methacrylate (PMMA) microfibers produced by electrospinning that used the processes and mechanical properties recently reported in detail by Alsmairat *et al* [61]. The employed PMMA solution was prepared by dissolving PMMA powders (50 000 in molecular weight, purchased from Sigma-Aldrich Co.) in acetone at a 23 wt.%. The electrospinning setup mainly consisted of a high voltage source, flow rate pump, syringe, and substrate. The needles have a diameter range of 80 to 100  $\mu\text{m}$ . Then, 10 kV are applied to the needle and the resulting electrostatic force overcomes the surface tension in the PMMA. Droplets in the form of Taylor cones are ejected from the needle and fly toward electrodes mounted on the substrate.

By setting the solution flow rate at 10  $\mu\text{l min}^{-1}$ , microfibers can be produced continually from the needle tip, and the fibers randomly accumulate between two electrodes placed 2 cm apart on the substrate. The manufactured fibers and fiber mat were dried inside a vacuum oven for 12 h.

The diameters of the fibers, their bonding, and the mat's porosity were characterized by using a high-resolution SEM (Supra 55 SEM from Zeiss). To avoid the electron charging effect, the to-be-inspected mat specimens were coated with a thin layer of conductive metal by using sputter coating. The mechanical properties of the individual fibers and fiber mats were characterized using a uniaxial micro-tensile testing purchased from ADMET Inc. The mesh sample ( $3 \times 5$  mm) was attached between the tensile tester screws, and the test was performed at 1  $\mu\text{m s}^{-1}$ .

### 2.2. Finite element model

To study the effect of interfiber bonding on the failure and rupture behavior of a mat, we created a  $2 \times 2$  mm 2D non-linear finite element model using randomly located and oriented fibers. Fibers were randomly added to the model until the ratio of non-occupied surface area by the fibers to the whole area reached the desired porosity of the mat. The porosity of the mat, expressed as a percentage, is defined as the ratio of the pores' surface area to the total surface area of the model. In our model, we set the diameter of the fibers to be 5.7  $\mu\text{m}$ , which was obtained from measurements. The diameters of the fibers inside the mat were measured using ImageJ software with the SEM image analysis. According to the measurements of 30 randomly selected fibers in the tested mat, the average diameter of fibers was found to be equal to  $5.7 \pm 0.6$   $\mu\text{m}$ . SEM images show the fibers have a uniform cross-section and a smooth surface. Fibers were modeled with the beam element (B21) in the Abaqus finite element

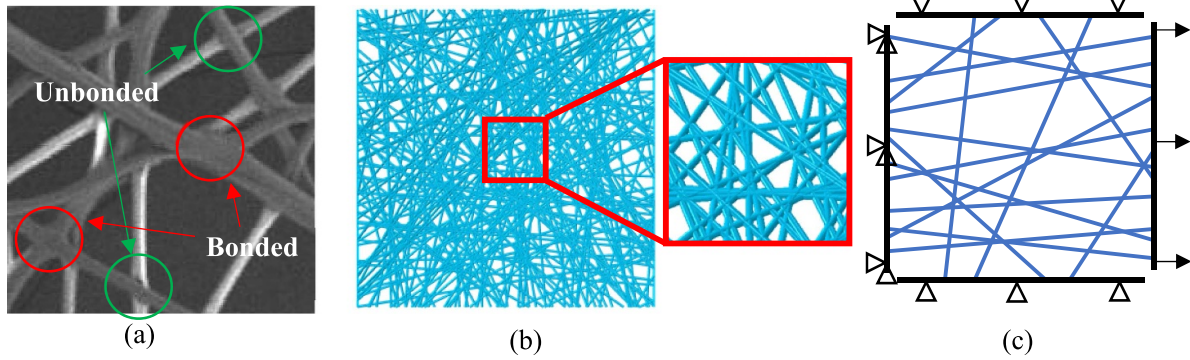


**Figure 1.** (a) A slice of a SEM image of the mat to identify unbonded and bonded cross-points. (b) Finite element model with random location and orientation of the fibers for the case with 25% porosity. (c) Boundary condition of the finite element model.

package. An auxiliary Python code was developed to find all cross-points of intersecting fibers to control the percentage of interfiber bonding. In this study, the bonding percentage is defined as the percentage ratio of the number of bonded cross-points to the total number of cross-points in the model. Five different cases with 5%, 10%, 25%, 50%, and 100% bonding between cross-points of fibers were considered. For the cases with 5%, 10%, 25%, and 50% bonding, 5%, 10%, 25%, and 50% of cross-points, respectively, were selected randomly and bonded together while the rest of the cross-points were free to move independently. For the case with 100% bonding, all cross-points of the intersecting fibers were bonded. The bonding concept in the model mimics the interfiber fusion (welding) in the experiment. A tie constraint was used to model perfect bonding (no relative motion) in the cross-points. Using ImageJ software, the porosity of the mat is calculated from the SEM image. A few slices of the SEM image were used to calculate the average porosity of the mat. The percentage of the bonding between fibers is calculated manually by counting the bonded and unbonded intersections. Figure 1(a) shows a slice of the SEM image of an electrospun PMMA mat. As figure 1(a) shows, the bonded and unbonded cross-points can be distinguished in the SEM image. In the bonded cross-points, fibers are fused. The porosity and the percentage of bonding between fibers were found to be roughly equal to 50%. Figures 1(b) and (c) show a sample finite element model with 50% porosity and the boundary condition of the model, respectively. The top and bottom edges of the model were assumed to have symmetric boundary conditions. The left edge of the model was fixed in ‘X’ and ‘Y’ directions, and the model was stretched uniaxially from the right edge.

A maximum strain criterion was established to determine a point when the fracture of fibers starts. Every fiber that reaches the maximum strain will begin to fail and tear. The equations (1)–(3) show the formulation of the fracture [62].

$$\varepsilon_D^{pl} = \left( \eta, \dot{\varepsilon}^{pl} \right) \quad (1)$$

$$\eta = -\frac{p}{q} \quad (2)$$

where the  $\varepsilon_D^{pl}$  is the equivalent plastic strain at the onset of damage, the  $\eta$  is the stress triaxiality,  $p$  is the pressure stress,  $q$  is the von Mises equivalent stress and  $\dot{\varepsilon}^{pl}$  demonstrates the equivalent plastic strain rate. The damage initiates when the following condition occurs:

$$\omega_D = \int \frac{d\varepsilon^{pl}}{\varepsilon_D^{pl} \left( \eta, \dot{\varepsilon}^{pl} \right)} = 1 \quad (3)$$

where  $\omega_D$  is a state variable that increases uniformly with plastic deformation.

### 3. Results and discussions

A (PMMA) mat is used in our study because of its availability, light weight, and low cost. It is a biocompatible polymer commonly used in medical applications [63, 64] and areas such as photovoltaic and triboelectric generators [65, 66]. A SEM image of the produced PMMA fiber mat manufactured by electrospinning is shown in figure 2(a). The SEM characterization showed the electrospun PMMA fibers possessed a solid uniform circular cross-section and their diameters could be controlled within a range from sub-micron to ~100 microns. Our recent tensile measurements, which are depicted by the stress-strain curve in figure 2(b), show that individual electrospun PMMA microfibers possess Young’s modulus of about 1.28 GPa and a tensile strength of about 16.31 MPa [61]. Figure 2(c) shows the representative stress–strain curve of one PMMA mat with Young’s modulus of about 8.21 MPa and tensile strength of about 0.14 MPa.

The elastic-plastic material property of a single fiber was obtained from the experiment and used in the FE model, figure 2(b). According to the experimental data and a trial-and-error method, the fracture strain and fracture energy for a single fiber were found to be 0.02 (mm/mm) and 0.0004 (N mm), respectively, to be used in FE model. The dashed line in figure 2(b) shows the fitted elastic-plastic behavior of the single fiber. To minimize the effect of randomness in the results, we ran three models with different random locations and orientation of fibers for each of the five cases. All of the results shown in this section are the average obtained from the three models

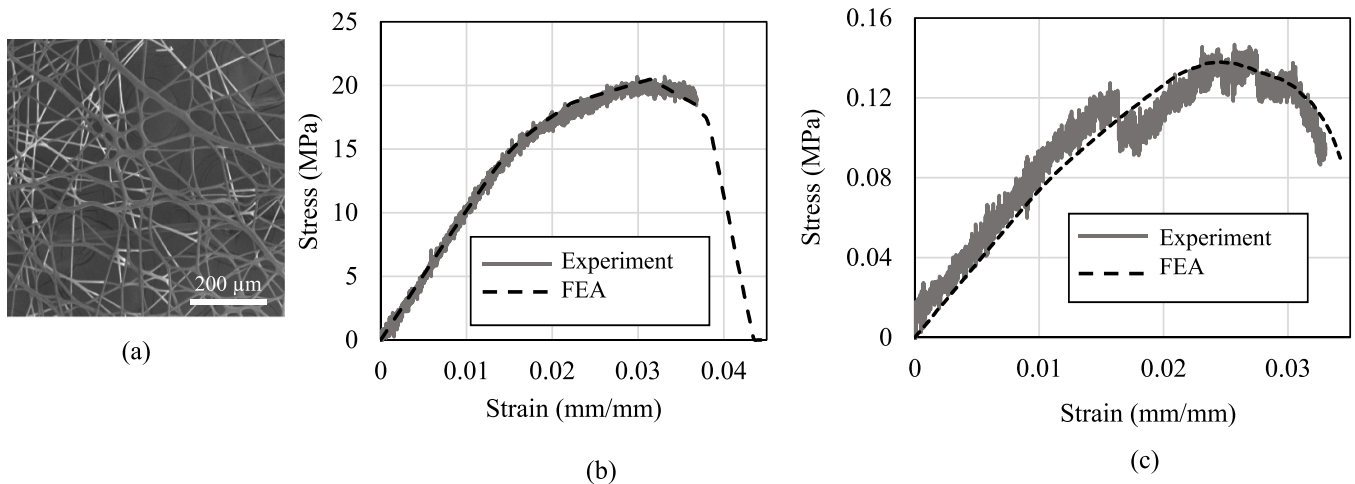


**Figure 2.** (a) SEM image of one electrospun Poly (methyl methacrylate) (PMMA) mat. (b) Representative engineering stress–strain curve of a single electrospun PMMA fiber (reproduced from [61]). © IOP Publishing Ltd. All rights reserved.) and the corresponding FE-fitted curve. (c) Representative engineering stress–strain curve of one electrospun PMMA mat from experimental tests and FE model with 50% porosity and 50% bonding. The model has 50% porosity and 50% interfiber bonding.

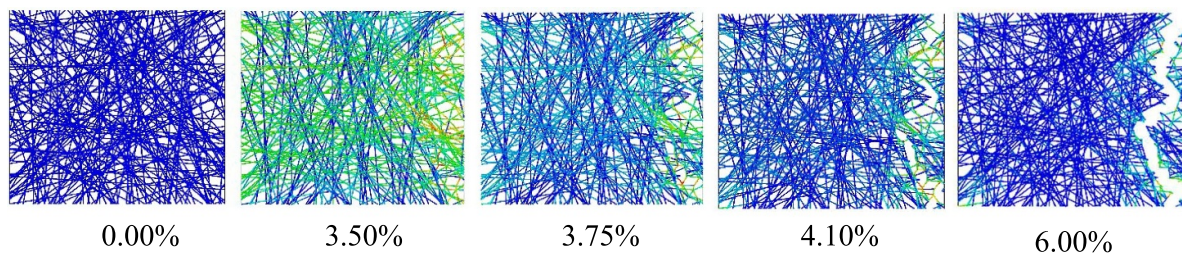
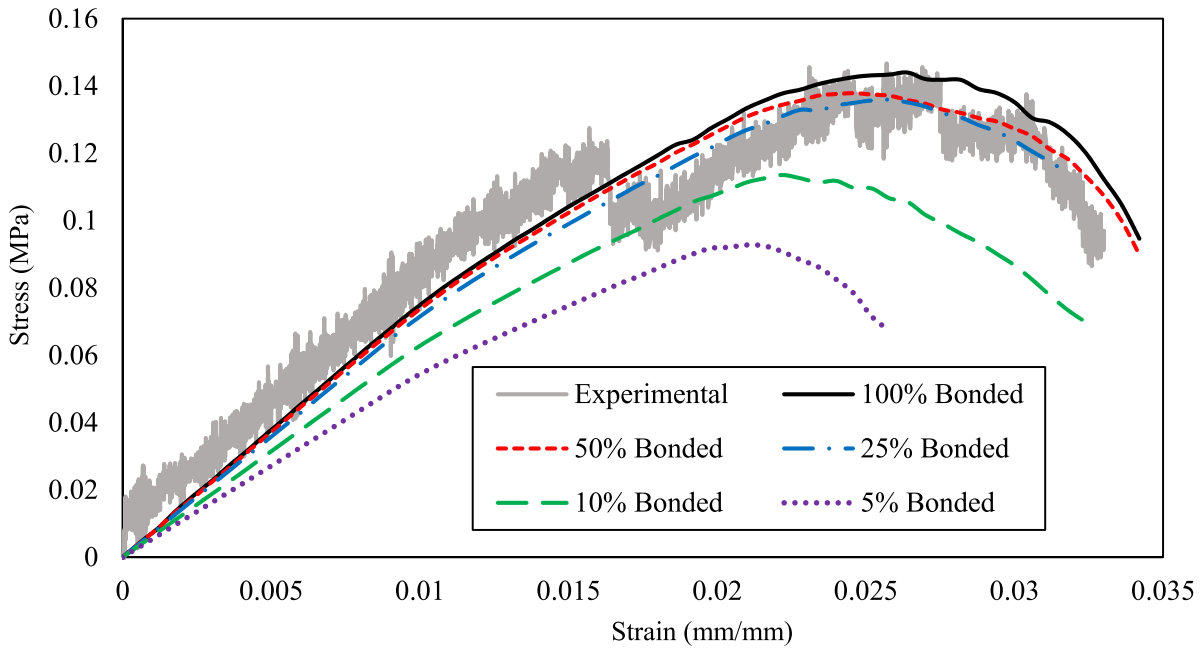


**Figure 3.** Evolution and progress of the fracture in a model with 50% porosity and 50% bonding. Numbers at the bottom of figures show the magnitude of the applied tensile strain. Blue to red shows greater stress.

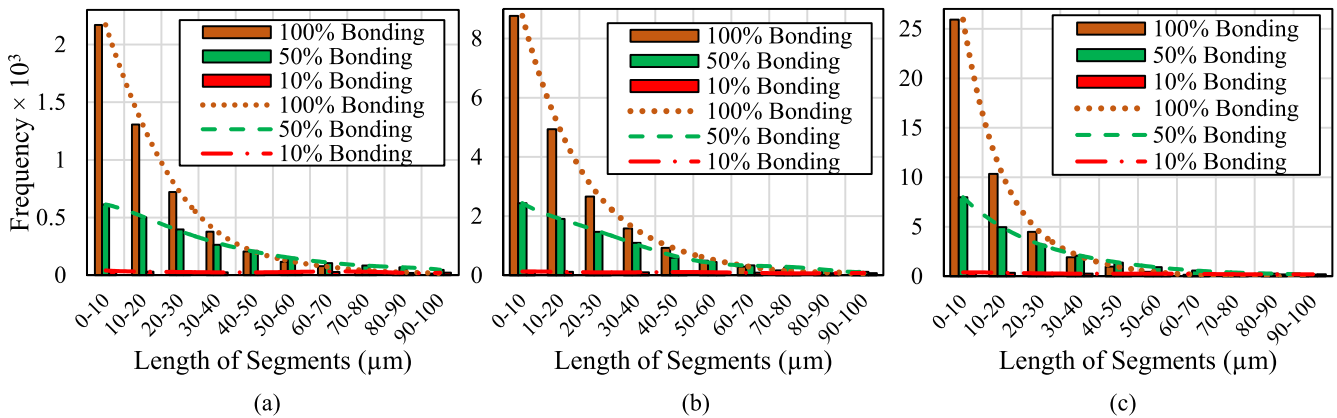
for each case. Figure 2(c) shows the stress–strain curve of the experimental test and FE model for a mat with 50% porosity and 50% bonding. From figure 2(c), the FE model predicts the rupture behavior of the mat with good accuracy. Figure 3 shows the stress distribution and the progress of the fracture in the mat for a model with 50% porosity and 50% bonding. The fracture starts at a small strain and progresses quickly. For the mat in figure 3, until a 3.5% strain there is no tearing, and the load is distributed throughout all the fibers. After a 3.5% strain, fracture begins at the right-bottom corner of the mat and propagates in such a way that by the time 4.1% strain is reached most of the mat is torn.

Figure 4 shows the average stress–strain curve of the mat for the cases with 5%, 10%, 25%, 50%, and 100% bonding and 50% porosity for all models. The effect of interfiber bonding on the mechanical behavior of the mat is obvious by comparing the lowest-percentage bonded case with the fully bonded case. For the case with 100% bonding, the elastic modulus of the mat is considerably higher than the cases with low percentages of bonding. In other words, interfiber bonding increases the stiffness of the mat [67]. This observation is in agreement with other experimental and modeling studies [43, 58, 67, 68]. Furthermore, fracture starts later for the case with 100% bonding. Therefore, bonding not only increases the stiffness of the mat, but also increases the fracture energy. This is because in

the cases with low percentages of bonding, fibers reach critical strain earlier than the case with 100% bonding. Thus, the fracture of fibers starts with a smaller strain for the cases with lower percentages of bonding. Interestingly, there are no significant differences in the mechanical behavior of cases with 100% and 50% bonding. This result is in agreement with the MD model of the behavior of electrospun nanofiber mats with the fiber–fiber fusion and van der Waals interaction at nano-scale [28]. This observation can be explained by the different responses of the elastic modulus of the mat in affine and non-affine deformation conditions. In dense fibrous networks (low porosity), the deformation is approximately affine [69] and the mat behaves as a nearly homogeneous material, while deformation is highly non-affine in low-density (high porosity) [70, 71]. Shahsavari *et al* [72] showed that the elastic modulus is independent of the cross-linking density at the affine limit, but is very sensitive to this parameter in the non-affine regime. Increasing the bond density in a predefined porosity reduces the fiber segment length, which causes fibers to deform axially rather than bend [59]. Therefore, the high percentage of the bonding in a predefined porosity shifts the mat to the affine deformation, and consequently bonding loses its effectiveness. Figure 4 makes clear that a 50% porosity, increasing the bonding percentage from 5% to 10% significantly increases the elastic modulus, while increasing the bonding percentage from



**Figure 4.** Stress–strain curve of the mat with 0%, 10%, 25%, 50%, and 100% bonding in cross-points. The porosity of all models is 50%.



**Figure 5.** Histogram of length of segments of fibers for cases with (a) 75% porosity, (b) 50% porosity, and (c) 25% porosity.

50% to 100% has a negligible effect. As a result, the effectiveness of the interfiber bonding is dependent on the porosity of the mat. The transformation between affine and non-affine deformation can be characterized by measuring the length of segments in the different percentage of bonding for different porosities, figure 5. Segment length is defined as the distance between the two connected bonded cross-points. As seen in figure 5, at any predefined porosity, increasing the percentage of bonding produces many smaller segments. As the result, small segments intrinsically prefer to be stretched and rotated rather than bent, and consequently the mat tends to have the affine deformation. As it is clear, at 25% porosity, there are many more small segments than at 50% and 75% porosities. The low density of interfiber bonding in a predefined porosity produces scatter locations for the stress concentration, while a high density of interfiber bonding removes stress concentrations and shifts the mat to isotropic material behavior. Therefore, as figure 4 shows, a mat with a low density of

interfiber bonding fails in the smaller strains than the mat with a high density of interfiber bonding.

Figure 4 also indicates that the effect of interfiber bonding on the mechanical behavior of the mat noticeably decreases in bonding percentage beyond 25%. The stress–strain curve of the mats with different percentages of bonding shows that for low interfiber bonding the mechanical behavior of the mat is highly dependent on the percentage of interfiber bonding, while this dependency decreases quickly as the percentage of bonding increases. This result is in agreement with the recent study by Theng *et al* [73]. This study showed that the effect of cross-link percentage (bonding percentage) in a predefined porosity diminishes enormously after a cross-link percentage threshold of 30%.

Results in figure 4 can only be applied to the specific porosity (50%) of the mat. It is expected that the effectiveness of the interfiber bonding can be a function of the porosity. Figure 6 shows the effect of bonding on the mechanical behavior of the

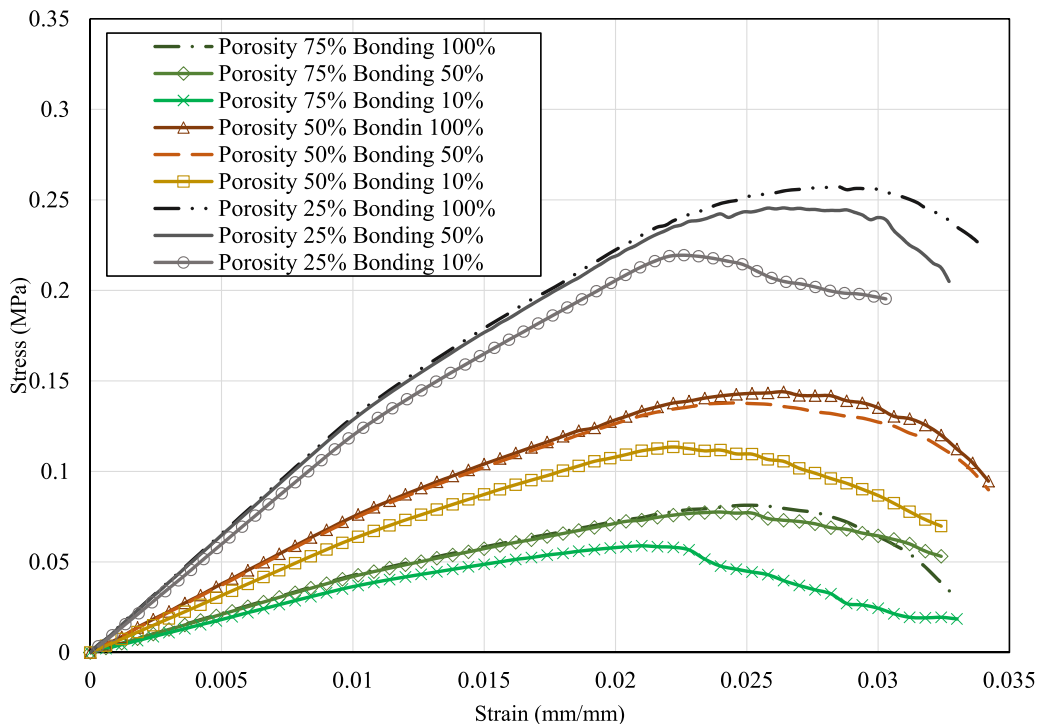


**Figure 6.** Effect of bonding on the mechanical behavior of the mat at different porosities.

mat at different porosities. First, as expected, mats with low porosity (large density of fibers) are stiffer and stronger than more porous mats [43]. As porosity increases, the stiffness of the mat decreases fairly linearly. By comparing the 100% bonding case with 25%, 50%, and 75% porosity, we can see that all cases start to tear at the same strain, relatively equal to 0.028 (mm/mm). This result indicates that porosity has a negligible effect on the maximum elongation of the mat in a fixed interfiber bonding percentage. This observation agrees with the modeling study [58], and with the experimental findings of [74] where while the elastic modulus, yield stress, and strength were considerably dependent on the porosity, the yield strain and strain to failure were independent. Goutianos *et al* [58] showed that an increase in the fiber volume fraction (reduction in porosity) and bond density has a minor effect on the strain to failure. Figure 6 shows that the interfiber bonding is more effective at the enhancing elastic modulus in higher porosities than lower porosities. By decreasing the percentage of bonding to 10% from 100%, the elastic modulus of the mat decreases by 8.45%, 16.17%, and 20.44% for the cases with 25%, 50%, and 75% porosity, respectively.

Figure 7 shows the dependency of the elastic modulus of the mat to the bonding density. Bonding density is defined as the number of bonded cross-points in a unit area. Marked points show the percentage of bonding. Increasing bond density for any porosity increases the elastic modulus of the mat. However, as discussed before, for each porosity there is a threshold for the density of bonding at which bonding loses its effectiveness. Bonding density is dependent on the defined porosity as well as the percentage of the bonding.

Figure 8 shows the dependency of the ultimate strength and toughness of the mat to the bonding density. Toughness

(fracture energy) of the mat is defined as the surface area below the stress-strain curve up to the failure strain. Toughness is the ability of the mat to absorb energy and plastically deform before rupturing. Similar to the elastic modulus, increasing the bonding density for different porosities increases the ultimate strength and the toughness of the mat. However, over-bonding cannot enhance the ultimate strength and toughness, and there will be a plateau state. The plateau state occurs marginally in a higher percentage of the bonding for a mat with the low porosity (25%) than the other higher porosities.

Finally, it is worth mentioning that the initial isotropy and the disordered networks of the mat with point contact between the crossing random fibers under the tension forms a highly oriented fibrous bundle with side contact between the aligned fibers [75]. This rearrangement results in a higher strain for the fibers that are mostly aligned in a tension axis rather than other fibers [76].

Similar to other computational studies, there are a few limitations in this study; (1) perfectly bonding condition without debonding was assumed for the fused cross-points. In reality, if the bonding strength is not enough, bond failures and fractures can be observed [68, 77]. Therefore, not only the percentage of bonding but also bond strength can affect the mechanical behavior of fibrous nonwoven materials. Bond damage has been identified as an important damage mechanism in the different types of fibrous non-wovens [78–80]; (2) only straight fibers were used in this study, while it has been shown that the curliness or curvature of fibers affects the mechanical properties of mats [32, 76, 81]. (3) The friction between unbonded and contacting fibers has not been considered in the models. In fact, there is slippage

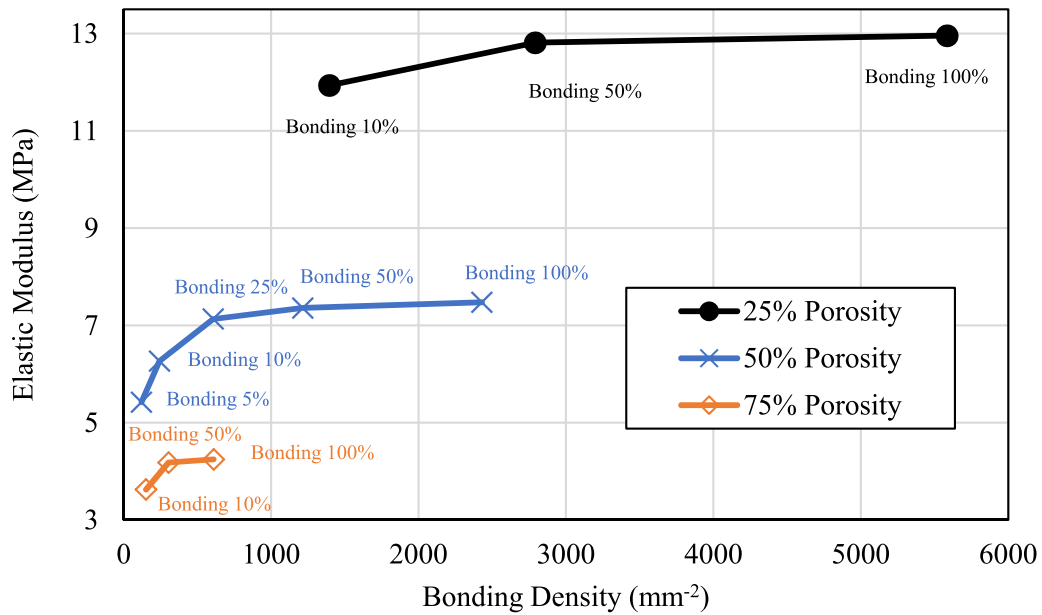


Figure 7. Effect of bonding density on the elastic modulus of the mat in different porosities and the percentage of the bonding.

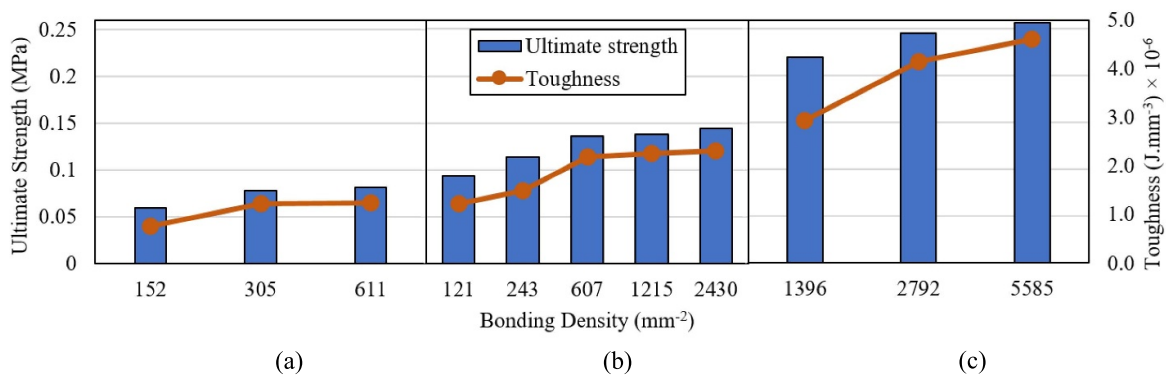


Figure 8. Effect of bonding density on ultimate strength and toughness of the mat for the cases with (a) 75% porosity, (b) 50% porosity, and (c) 25% porosity.

between the unbonded and contacting fibers [82]. Studying the aforementioned limitations could be an interest for future studies.

#### 4. Conclusion

In this study, we proposed a new multiscale finite element model to investigate the effect of the interfiber bonding in different porosities on the rupture behavior of the electrospun fibrous mat. The results show that increasing interfiber bonding increases the stiffness and toughness of the mat. The sensitivity of the mechanical behavior of the mat to bonding decreases by increasing the percentage of the bonding. A large percentage of bonding at a predefined porosity shifts the mat to an affine deformation and consequently, bonding loses its effectiveness. Furthermore, bonding increases the maximum possible elongation of the mat. The study provides an insight into the fracture of fibrous mats that can be useful for the application of electrospun mats in technologies such

as nanomesh on-skin electronics [83], artificial extracellular matrices [84], and wound dressings [85].

#### Acknowledgments

P C and M J R acknowledge the support from Binghamton University’s start-up research funding. The PMMA fiber mats were manufactured using an electrospay printer in Professor P R Chiarot’s group. O Q A and C H K acknowledge financial support from the National Institute of Health under Grant No. 1R01DC017720.

#### Data availability

The data that support the findings of this study are available from the corresponding author upon reasonable request.

## ORCID iDs

Changhong Ke  <https://orcid.org/0000-0002-5170-9859>  
 Mir Jalil Razavi  <https://orcid.org/0000-0002-8421-9688>

## References

- [1] Xue J, Wu T, Dai Y and Electrospinning X Y 2019 Electrospun nanofibers: methods, materials, and applications *Chem. Rev.* **119** 5298–415
- [2] Bhardwaj N and Kundu S C 2010 Electrospinning: a fascinating fiber fabrication technique *Biotechnol. Adv.* **28** 325–47
- [3] Ding B, Wang X and Yu J 2019 *Electrospinning: Nanofabrication and Applications* (Amsterdam: Elsevier)
- [4] Mohamadzadehmoghadam S, Dong Y and Davies I J 2016 Modeling electrospun nanofibers: an overview from theoretical, empirical, and numerical approaches *Int. J. Polym. Mater. Polym. Biomater.* **65** 901–15
- [5] Leach M K, Feng Z-Q, Tuck S J and Corey J M 2011 Electrospinning fundamentals: optimizing solution and apparatus parameters *J. Vis. Exp.* **47** 2494
- [6] Cacciotti I, House J N, Mazzuca C, Valentini M, Madau F, Palleschi A, Straffi P and Nanni F 2015 Neat and GNPs loaded natural rubber fibers by electrospinning: manufacturing and characterization *Mater. Des.* **88** 1109–18
- [7] Wu S-H and Qin X-H 2013 Uniaxially aligned polyacrylonitrile nanofiber yarns prepared by a novel modified electrospinning method *Mater. Lett.* **106** 204–7
- [8] İçoğlu H İ, Ceylan Ş, Yıldırım B, Topalbekiroğlu M and Kılıç A 2020 Production of aligned electrospun polyvinyl alcohol nanofibers via parallel electrode method *J. Text. Inst.* **1–10**
- [9] Leon-Valdivieso C Y, Garcia-Garcia A, Legallais C and Bedoui F 2020 Electrospinning of biomedically relevant multi-region scaffolds: from honeycomb to randomly-oriented microstructure *Polymer* **202** 122606
- [10] Shabafrooz V, Mozafari M, Vashae D and Tayebi L 2014 Electrospun nanofibers: from filtration membranes to highly specialized tissue engineering scaffolds *J. Nanosci. Nanotechnol.* **14** 522–34
- [11] Lu P and Ding B 2008 Applications of electrospun fibers *Recent Pat. Nanotechnol.* **2** 169–82
- [12] Heikkilä P, Taipale A, Lehtimäki M and Harlin A 2008 Electrospinning of polyamides with different chain compositions for filtration application *Polym. Eng. Sci.* **48** 1168–76
- [13] Mirjalili M and Zohoori S 2016 Review for application of electrospinning and electrospun nanofibers technology in textile industry *J. Nanostruct. Chem.* **6** 207–13
- [14] Duan Y, Jia J, Wang S-H, Yan W, Jin L and Wang Z-Y 2007 Preparation of antimicrobial poly( $\epsilon$ -caprolactone) electrospun nanofibers containing silver-loaded zirconium phosphate nanoparticles *J. Appl. Polym. Sci.* **106** 1208–14
- [15] Bianco A, Calderone M and Electrospun C I 2013 PHBV/PEO co-solution blends: microstructure, thermal and mechanical properties *Mater. Sci. Eng. C* **33** 1067–77
- [16] Ding J, Zhang J, Li J, Li D, Xiao C, Xiao H, Yang H, Zhuang X and Chen X 2019 Electrospun polymer biomaterials *Prog. Polym. Sci.* **90** 1–34
- [17] Min L, Pan H, Chen S, Wang C, Wang N, Zhang J, Cao Y, Chen X and Hou X 2019 Recent progress in bio-inspired electrospun materials *Compos. Commun.* **11** 12–20
- [18] Pai C-L, Boyce M C and Rutledge G C 2011 Mechanical properties of individual electrospun PA 6 (3)T fibers and their variation with fiber diameter *Polymer* **52** 2295–301
- [19] Croisier F, Duwez A-S, Jérôme C, Léonard A F, van der Werf K O, Dijkstra P J and Binnink M L 2012 Mechanical testing of electrospun PCL fibers *Acta Biomater.* **8** 218–24
- [20] Carlisle C R, Coulais C and Guthold M 2010 The mechanical stress–strain properties of single electrospun collagen type I nanofibers *Acta Biomater.* **6** 2997–3003
- [21] Naraghi M, Arshad S N and Chasiotis I 2011 Molecular orientation and mechanical property size effects in electrospun polyacrylonitrile nanofibers *Polymer* **52** 1612–8
- [22] Wong S-C, Baji A and Leng S 2008 Effect of fiber diameter on tensile properties of electrospun poly( $\epsilon$ -caprolactone) *Polymer* **49** 4713–22
- [23] Stylianopoulos T, Kokonou M, Michael S, Tryfonos A, Rebolz C, Odysseos A D and Doumanidis C 2012 Tensile mechanical properties and hydraulic permeabilities of electrospun cellulose acetate fiber meshes *J. Biomed. Mater. Res. B* **100B** 2222–30
- [24] Choong L T S, Khan Z and Rutledge G C 2014 Permeability of electrospun fiber mats under hydraulic flow *J. Membr. Sci.* **451** 111–6
- [25] Sampson W W 2003 A multiplanar model for the pore radius distribution in isotropic near-planar stochastic fibre networks *J. Mater. Sci.* **38** 1617–22
- [26] Bagherzadeh R, Latifi M, Najar S S and Kong L 2014 Experimental verification of theoretical prediction of fiber to fiber contacts in electrospun multilayer nano-microfibrous assemblies: effect of fiber diameter and network porosity *J. Ind. Text.* **43** 483–95
- [27] Cacciotti I, Calderone M and Bianco A 2013 Tailoring the properties of electrospun PHBV mats: co-solution blending and selective removal of PEO *Eur. Polym. J.* **49** 3210–22
- [28] Wei X, Xia Z, Wong S C and Baji A 2009 Modelling of mechanical properties of electrospun nanofibre network *Int. J. Exp. Comput. Biomech.* **1** 45
- [29] Buell S, Rutledge G C and Vliet K J V 2010 Predicting polymer nanofiber interactions via molecular simulations *ACS Appl. Mater. Interfaces* **2** 1164–72
- [30] Wu X-F and Dzenis Y A 2007 Adhesive contact in filaments *J. Phys. D: Appl. Phys.* **40** 4276–80
- [31] Stylianopoulos T, Bashur C A, Goldstein A S, Guelcher S A and Barocas V H 2008 Computational predictions of the tensile properties of electrospun fibre meshes: effect of fibre diameter and fibre orientation *J. Mech. Behav. Biomed. Mater.* **1** 326–35
- [32] Pai C-L, Boyce M C and Rutledge G C 2011 On the importance of fiber curvature to the elastic moduli of electrospun nonwoven fiber meshes *Polymer* **52** 6126–33
- [33] Rizvi M S, Kumar P, Katti D S and Pal A 2012 Mathematical model of mechanical behavior of micro/nanofibrous materials designed for extracellular matrix substitutes *Acta Biomater.* **8** 4111–22
- [34] Rizvi M S and Pal A 2014 Statistical model for the mechanical behavior of the tissue engineering non-woven fibrous matrices under large deformation *J. Mech. Behav. Biomed. Mater.* **37** 235–50
- [35] Vatankhah E, Semnani D, Prabhakaran M P, Tadayon M, Razavi S and Ramakrishna S 2014 Artificial neural network for modeling the elastic modulus of electrospun polycaprolactone/gelatin scaffolds *Acta Biomater.* **10** 709–21
- [36] Polak-Krasna K, Georgiadis A and Heikkilä P 2015 Mechanical characterisation and modelling of electrospun materials for biomedical applications *2015 IEEE Int. Symp. on Medical Measurements and Applications (MeMeA) Proc.* pp 507–11
- [37] Yin Y and Xiong J 2018 Finite element analysis of electrospun nanofibrous mats under biaxial tension *Nanomaterials* **8** 348
- [38] Yin Y, Pan Z and Xiong J 2018 A tensile constitutive relationship and a finite element model of electrospun nanofibrous mats *Nanomaterials* **8** 29

- [39] Koh C T, Low C Y and bin Yusof Y 2015 Structure-property relationship of bio-inspired fibrous materials *Procedia Comput. Sci.* **76** 411–6
- [40] Farukh F, Demirci E, Sabuncuoglu B, Acar M, Pourdeyhimi B and Silberschmidt V V 2014 Numerical analysis of progressive damage in nonwoven fibrous networks under tension *Int. J. Solids Struct.* **51** 1670–85
- [41] Driscoll T P, Nerurkar N L, Jacobs N T, Elliott D M and Mauck R L 2011 Fiber angle and aspect ratio influence the shear mechanics of oriented electrospun nanofibrous scaffolds *J. Mech. Behav. Biomed. Mater.* **4** 1627–36
- [42] Deogekar S and Picu R C 2018 On the strength of random fiber networks *J. Mech. Phys. Solids* **116** 1–16
- [43] Zhang M, Chen Y, Chiang F, Gouma P I and Wang L 2019 Modeling the large deformation and microstructure evolution of nonwoven polymer fiber networks *J. Appl. Mech.* **86** 011010
- [44] Lee S J, Oh S H, Liu J, Soker S, Atala A and Yoo J J 2008 The use of thermal treatments to enhance the mechanical properties of electrospun poly( $\epsilon$ -caprolactone) scaffolds *Biomaterials* **29** 1422–30
- [45] Wang S-X, Yang L, Stubbs L P, Li X and He C 2013 Lignin-derived fused electrospun carbon fibrous mats as high performance anode materials for lithium ion batteries *ACS Appl. Mater. Interfaces* **5** 12275–82
- [46] Shi Z, Jin G, Wang J and Zhang J 2017 Free-standing, welded mesoporous carbon nanofibers as anode for high-rate performance Li-ion batteries *J. Electroanal. Chem.* **795** 26–31
- [47] Zillohu A, Alissawi N, Abdelaziz R and Elbahri M 2014 Thermo-plasmonics for localized graphitization and welding of polymeric nanofibers *Materials* **7** 323–32
- [48] Huang L, Manickam S S and McCutcheon J R 2013 Increasing strength of electrospun nanofiber membranes for water filtration using solvent vapor *J. Membr. Sci.* **436** 213–20
- [49] Li H, Zhu C, Xue J, Ke Q and Xia Y 2017 Enhancing the mechanical properties of electrospun nanofiber mats through controllable welding at the cross points *Macromol. Rapid Commun.* **38** 1600723
- [50] Jang S-Y, Seshadri V, Khil M-S, Kumar A, Marquez M, Mather P T and Sotzing G A 2005 Welded electrochromic conductive polymer nanofibers by electrostatic spinning *Adv. Mater.* **17** 2177–80
- [51] Wang W, Jin X, Zhu Y, Zhu C, Yang J, Wang H and Lin T 2016 Effect of vapor-phase glutaraldehyde crosslinking on electrospun starch fibers *Carbohydr. Polym.* **140** 356–61
- [52] Farukh F, Demirci E, Acar M, Pourdeyhimi B and Silberschmidt V V 2013 Meso-scale deformation and damage in thermally bonded nonwovens *J. Mater. Sci.* **48** 2334–45
- [53] Farukh F, Demirci E, Sabuncuoglu B, Acar M, Pourdeyhimi B and Silberschmidt V V 2012 Numerical modelling of damage initiation in low-density thermally bonded nonwovens *Comput. Mater. Sci.* **64** 112–5
- [54] Sozumert E, Farukh F, Sabuncuoglu B, Demirci E, Acar M, Pourdeyhimi B and Silberschmidt V V 2020 Deformation and damage of random fibrous networks *Int. J. Solids Struct.* **184** 233–47
- [55] Wilbrink D V, Beex L A A and Peerlings R H J 2013 A discrete network model for bond failure and frictional sliding in fibrous materials *Int. J. Solids Struct.* **50** 1354–63
- [56] Luo G, Shi L, Li M, Zhong Y, He X and Wang J 2018 Ductile–brittle transition in transverse isotropic fibrous networks *Appl. Phys. Lett.* **112** 051904
- [57] Koh C T and Oyen M L 2015 Toughening in electrospun fibrous scaffolds *APL Mater.* **3** 014908
- [58] Goutianos S, Mao R and Peijs T 2018 Effect of inter-fibre bonding on the fracture of fibrous networks with strong interactions *Int. J. Solids Struct.* **136–137** 271–8
- [59] Chen N and Silberstein M N 2018 Determination of bond strengths in non-woven fabrics: a combined experimental and computational approach *Exp. Mech.* **58** 343–55
- [60] Chen N and Silberstein M N 2019 A micromechanics-based damage model for non-woven fiber networks *Int. J. Solids Struct.* **160** 18–31
- [61] Alsmairat O Q, Gou F, Dmuchowski C M, Chiarot P R, Park C, Miles R N and Ke C 2020 Quantifying the interfacial load transfer in electrospun carbon nanotube polymer nanocomposite microfibers by using *in situ* Raman micromechanical characterization techniques *J. Phys. D: Appl. Phys.* **53** 365302
- [62] 2013 *Abaqus Analysis User's Manual, Version 6.13* (Johnston, RI: Dassault System Simulia Corp.)
- [63] Glasgow K C and Dhara D 2008 An overview of the biocompatibility of polymeric surfaces *Polymers for Biomedical Applications* vol 977, ed A Mahapatro and A S Kulshrestha (Washington, DC: American Chemical Society) pp 268–82
- [64] Maitz M F 2015 Applications of synthetic polymers in clinical medicine *Biosurf. Biotribol.* **1** 161–76
- [65] Yang H, Huang M, Wu J, Lan Z, Hao S and Lin J 2008 The polymer gel electrolyte based on poly(methyl methacrylate) and its application in quasi-solid-state dye-sensitized solar cells *Mater. Chem. Phys.* **110** 38–42
- [66] Busolo T, Ura D P, Kim S K, Marzec M M, Bernasik A, Stachewicz U and Kar-Narayan S 2019 Surface potential tailoring of PMMA fibers by electrospinning for enhanced triboelectric performance *Nano Energy* **57** 500–6
- [67] Chavoshnejad P and Razavi M J 2020 Effect of the interfiber bonding on the mechanical behavior of electrospun fibrous mats *Sci. Rep.* **10** 7709
- [68] Choi -S-S, Lee S G, Joo C W, Im S S and Kim S H 2004 Formation of interfiber bonding in electrospun poly(etherimide) nanofiber web *J. Mater. Sci.* **39** 1511–3
- [69] Lee D H and Carnaby G A 1992 Compressional energy of the random fiber assembly: part I: theory *Text. Res. J.* **62** 185–91
- [70] Wilhelm J and Frey E 2003 Elasticity of stiff polymer networks *Phys. Rev. Lett.* **91** 108103
- [71] Shahsavari A and Picu R C 2012 Model selection for athermal cross-linked fiber networks *Phys. Rev. E* **86** 011923
- [72] Shahsavari A S and Picu R C 2013 Elasticity of sparsely cross-linked random fibre networks *Phil. Mag. Lett.* **93** 356–61
- [73] Theng K C and Chung S M 2020 Effects of microstructure architecture on the fracture of fibrous materials *Int. J. Integr. Eng.* **12** 138–43
- [74] Henriksson M, Berglund L A, Isaksson P, Lindström T and Nishino T 2008 Cellulose nanopaper structures of high toughness *Biomacromolecules* **9** 1579–85
- [75] Li J, Nie C, Duan B, Zhao X, Lu H, Yin W, Li Y and He X 2017 Tensile performance of silica-based electrospun fibrous mats *J. Non-Cryst. Solids* **470** 184–8
- [76] Domaschke S, Zündel M, Mazza E and Ehret A E 2019 A 3D computational model of electrospun networks and its application to inform a reduced modelling approach *Int. J. Solids Struct.* **158** 76–89
- [77] Torgnysdotter A, Kulachenko A, Gradin P and Wågberg L 2007 The link between the fiber contact zone and the physical properties of paper: a way to control paper properties *J. Compos. Mater.* **41** 1619–33
- [78] Ridruejo A, González C and LLorca J 2011 Micromechanisms of deformation and fracture of polypropylene nonwoven fabrics *Int. J. Solids Struct.* **48** 153–62
- [79] Chen N, Koker M K A, Uzun S and Silberstein M N 2016 *In-situ* x-ray study of the deformation mechanisms of non-woven polypropylene *Int. J. Solids Struct.* **97–98** 200–8

- [80] Isaksson P, Gradin P A and Kulachenko A 2006 The onset and progression of damage in isotropic paper sheets *Int. J. Solids Struct.* **43** 713–26
- [81] Kumar V and Rawal A 2017 Elastic moduli of electrospun mats: importance of fiber curvature and specimen dimensions *J. Mech. Behav. Biomed. Mater.* **72** 6–13
- [82] Negi V and Picu R C 2019 Mechanical behavior of nonwoven non-crosslinked fibrous mats with adhesion and friction *Soft Matter* **15** 5951–64
- [83] Brown M S, Mendoza M, Chavoshnejad P, Razavi M J, Mahler G J and Koh A 2020 Electronic-ECM: a permeable microporous elastomer for an advanced bio-integrated continuous sensing platform *Adv. Mater. Technol.* **5** 2000242
- [84] Molnar K, Juriga D, Nagy P M, Sinko K, Jedlovszky-Hajdu A and Zrinyi M 2014 Electrospun poly(aspartic acid) gel scaffolds for artificial extracellular matrix: electrospun poly(aspartic acid) gel scaffolds *Polym. Int.* **63** 1608–15
- [85] Liu Y, Zhou S, Gao Y and Zhai Y 2019 Electrospun nanofibers as a wound dressing for treating diabetic foot ulcer *Asian J. Pharm. Sci.* **14** 130–43